

# Projected changes in wave climate from a multi-model ensemble

Mark A. Hemer<sup>1\*</sup>, Yalin Fan<sup>2</sup>, Nobuhito Mori<sup>3</sup>, Alvaro Semedo<sup>4,5</sup> and Xiaolan L. Wang<sup>6</sup>

**Future changes in wind-wave climate have broad implications for the operation and design of coastal, near- and off-shore industries and ecosystems, and may further exacerbate the anticipated vulnerabilities of coastal regions to projected sea-level rise<sup>1,2</sup>. However, wind waves have received little attention in global assessments of projected future climate change. We present results from the first community-derived multi-model ensemble of wave-climate projections. We find an agreed projected decrease in annual mean significant wave height ( $H_S$ ) over 25.8% of the global ocean area. The area of projected decrease is greater during boreal winter (January–March, mean; 38.5% of the global ocean area) than austral winter (July–September, mean; 8.4%). A projected increase in annual mean  $H_S$  is found over 7.1% of the global ocean, predominantly in the Southern Ocean, which is greater during austral winter (July–September; 8.8%). Increased Southern Ocean wave activity influences a larger proportion of the global ocean as swell propagates northwards into the other ocean basins, observed as an increase in annual mean wave period ( $T_M$ ) over 30.2% of the global ocean and associated rotation of the annual mean wave direction ( $\theta_M$ ). The multi-model ensemble is too limited to systematically sample total uncertainty associated with wave-climate projections. However, variance of wave-climate projections associated with study methodology dominates other sources of uncertainty (for example, climate scenario and model uncertainties).**

There is increasing evidence for climate-driven historical variability of wind-wave climate over at least the satellite altimeter era<sup>3–6</sup> with trends in wave height seen in observing ship records over the past half-century<sup>7</sup>. Observed variability in wave climate is attributable to changes in global marine wind fields (for example, refs 6,8) and with projected future changes in these winds<sup>9</sup>, climate-driven changes in wave climate are anticipated. However, coupled atmosphere–ocean general circulation models (GCMs) generally do not yet include wind-wave-dependent parameterizations<sup>10</sup>, and wave parameters are therefore not available amongst the standard suite of climate variables used to characterize the climate system<sup>2,11</sup>. As a result, the understanding of projected changes in wave climate is limited relative to other climatological parameters such as temperature, precipitation or sea level.

A growing number of studies have considered how global wave climate may respond to projected future climate scenarios with increased greenhouse-gas concentrations<sup>12–14</sup> (Y. F. *et al.* and A. S. *et al.* manuscripts in preparation). These studies have been carried out independently, using different methods to investigate projected future wave-climate changes. Within each individual

study, only a limited number of climate model simulations were investigated owing to limited study scope and/or availability of suitable climate model data. Individual studies are therefore unable to fully quantify the uncertainty of projected changes in wave climate. Here, our primary aim is to use results contributed to the Coordinated Ocean Wave Climate Project<sup>11</sup> (COWCLIP) to quantitatively compare the magnitude of projected changes derived from five independent studies and to determine the level of agreement between available projections of wave climate. Four of the five contributions (ref. 13, Y. F. *et al.* (manuscript in preparation), ref. 14 and A. S. *et al.* (manuscript in preparation), hereafter MEA10, FEA12, HEA12 and SEA12, respectively) take a dynamical approach. In these studies, high-resolution atmospheric GCMs are used to dynamically downscale the results of a forcing atmosphere–ocean GCM. Surface winds from the high-resolution atmospheric model are then used to force a spectral wind-wave model. The fifth contribution<sup>12</sup> (WS06) uses a statistical approach to develop wave-climate projections, exploiting a relationship between mean sea-level pressure (MSLP) and  $H_S$ . Details of each contribution are given in the Supplementary Information.

Contributing studies<sup>12–14</sup> (Y. F. *et al.* and A. S. *et al.*, manuscripts in preparation) have assessed the performance of each model to represent the historical wave climate on an individual basis. Here, we assess model skill of each contribution using pattern correlation and root-mean-square deviations (r.m.s.d.) between model wave fields from the representative historical time-slice with wave reanalysis data (from ERA-Interim<sup>15</sup> and C-ERA40 (ref. 16)—see Supplementary Information). Model skill is strongly dependent on the approach of each study to develop wave-climate fields (which we term methodology), as shown by clustering of ensemble members from each study (Fig. 1). Methodology refers to whether the approach taken is dynamical (for example, HEA12, MEA10, FEA12 and SEA12) or statistical (for example, WS06), but also the specifics of the combination of downscaling atmospheric GCM and wave models used in dynamical studies, or the statistical model developed for statistical studies. The r.m.s.d. in  $H_S$  between the models and ERA-Interim and C-ERA40 is typically less than 0.6 m regardless of study, region of comparison (Global, G; Northern Hemisphere, NH; Equatorial, Eq; or Southern Hemisphere—see Methods for definition) or season (annual, January–March (JFM) or July–September (JAS) mean). The MEA10 member shows an  $H_S$  r.m.s.d. of 0.55 m, with the lowest  $H_S$  correlations in the ensemble of 0.45 (annual equatorial mean, relative to ERA-Interim; Fig. 1a) reflecting the large bias observed in this model in the equatorial region (see Supplementary Information). All other ensemble members exhibit high (>0.85)  $H_S$

<sup>1</sup>CSIRO Wealth from Oceans National Research Flagship and the Centre of Australian Weather and Climate Research: A Partnership between CSIRO and the Bureau of Meteorology, GPO Box 1538, Hobart, Tasmania 7001, Australia, <sup>2</sup>Princeton University/GFDL, Princeton, New Jersey 08536, USA, <sup>3</sup>Disaster Prevention Research Institute, Kyoto University, Kyoto 611-0011, Japan, <sup>4</sup>Escola Naval, CINAV, Lisbon 2810-001, Portugal, <sup>5</sup>Department of Earth Sciences, Uppsala University, Uppsala 752 36, Sweden, <sup>6</sup>Climate Research Division, Science and Technology Branch, Environment Canada, Toronto, Ontario, M3H 5T4, Canada. \*e-mail: mark.hemer@csiro.au.

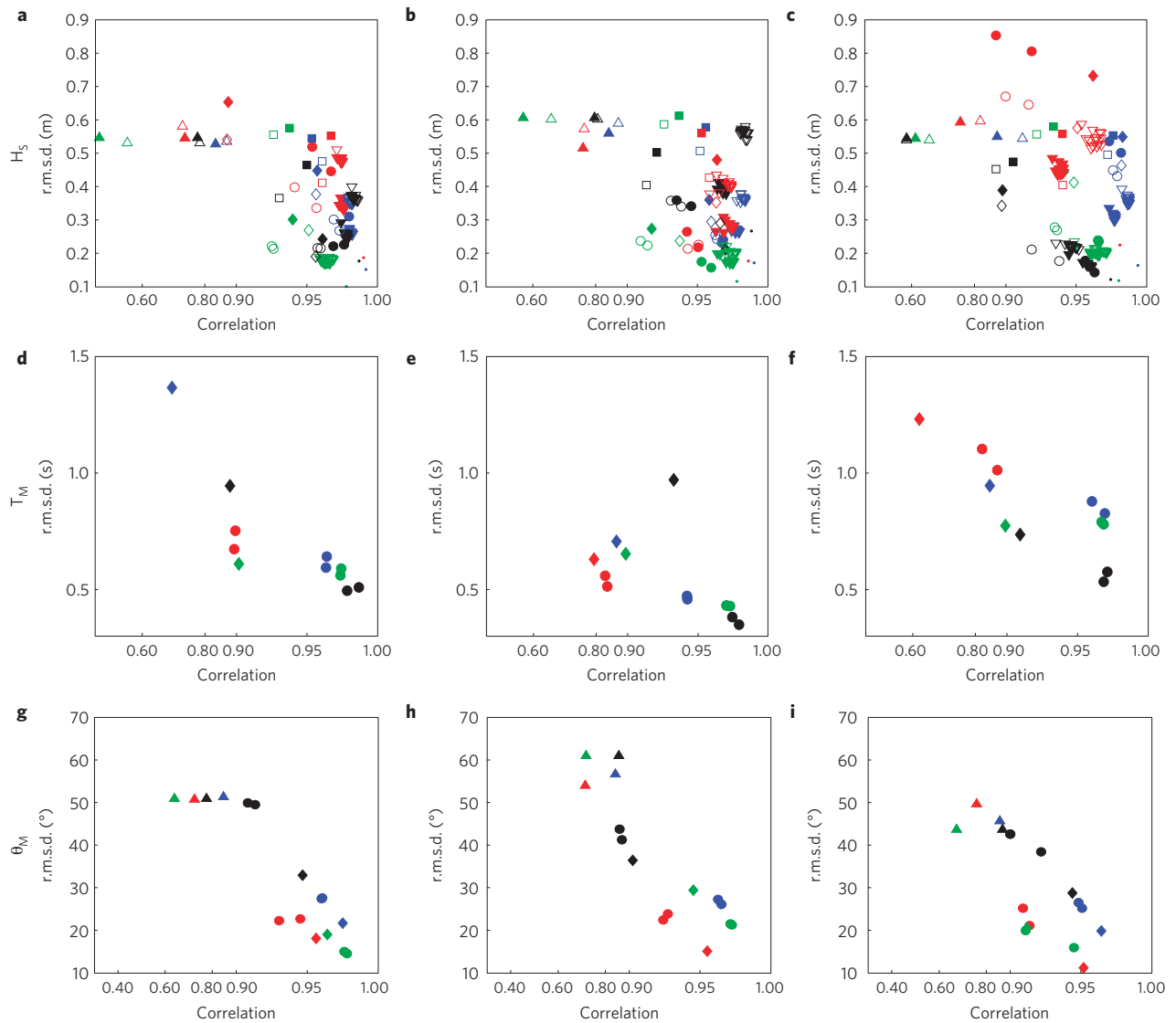


**Figure 1 | Correlation and r.m.s.d. of  $H_s$ ,  $T_M$  and  $\theta_M$  for models with respect to ERA-Interim and C-ERA40.** **a–i**, Left, centre and right plots show comparisons of annual, JFM and JAS, respectively. Global comparisons are indicated in blue, Southern Hemisphere in red, equatorial region in green and Northern Hemisphere in black. HEA12 runs (circles); MEA10 (uptriangles); FEA12 (diamonds); SEA12 (squares) and WS06 (downtriangles). Dots designate r.m.s.d. and correlation between ERA-Interim (filled markers) and C-ERA40 (open markers). Bias relative to ERA-Interim for each individual model is included in the Supplementary Information. Note the nonlinear scale on the abscissa of each subplot.

correlation with reanalyses (Fig. 1). WS06 ensemble members show closest agreement with reanalyses because they were produced using ERA-40 reanalysis sea-level pressure and  $H_s$  relationships, although r.m.s.d. up to 0.6 m is observed (JAS SH mean, relative to C-ERA40; Fig. 1c). A positive bias in SH  $H_s$  during JAS found in HEA12 ensemble members (see Supplementary Information) leads to the largest r.m.s.d. observed in the ensemble (0.8–0.85 m relative to ERA-Interim; Fig. 1c), but correlation remains relatively high (0.91 and 0.88). Further assessment of model skill including assessment of interannual variability bias and historical trends is given in the Supplementary Information.

Three of the five contributing groups (MEA10, FEA12 and HEA12) provided  $T_M$  and  $\theta_M$  fields for inter-comparison. Strong negative biases in  $T_M$  and strong zonal biases in  $\theta_M$  are observed in the MEA10 historical time-slices (see Supplementary Information). This is characteristic of strong dissipation of low-frequency (swell) waves in this model. As with  $H_s$ , the remaining members cluster by methodology, with a tendency for lower correlations/larger r.m.s.d. in the SH during the austral winter (JAS; Fig. 1f). These differences

are observed as a positive (negative)  $T_M$  bias in the SH in the HEA12 (FEA12) members (see Supplementary Information).

Correlation and r.m.s.d. values for  $\theta_M$  show a similar level of agreement as for  $T_M$ . Correlation values range between 0.62 (MEA12 Eq annual and JAS means; Fig. 1g) to 0.96 (HEA12 Eq annual mean; Fig. 1g). The values for the r.m.s.d. range from 11° (FEA12 SH JAS mean; Fig. 1i) to over 60° (MEA12 NH and Eq JFM mean; Fig. 1h). Both HEA12 and FEA12 models show similar characteristics with a bias of approximately 15° towards increased zonal (easterly) flow in the equatorial regions, and an increased southerly component in the Southern Ocean (see Supplementary Information).

Signals of projected change in  $H_s$  show agreement between models over considerable portions of the global ocean (Fig. 2). Changes in the multi-model annual mean  $H_s$  ( $\overline{H_s}$ ) show a consistent projected decrease among models over a larger area (25.8% of the global ocean) and consistent increases over a smaller area (7.1% of the global ocean; Table 1). Projected increases in  $\overline{H_s}$  are generally limited to the Southern Ocean, associated with a

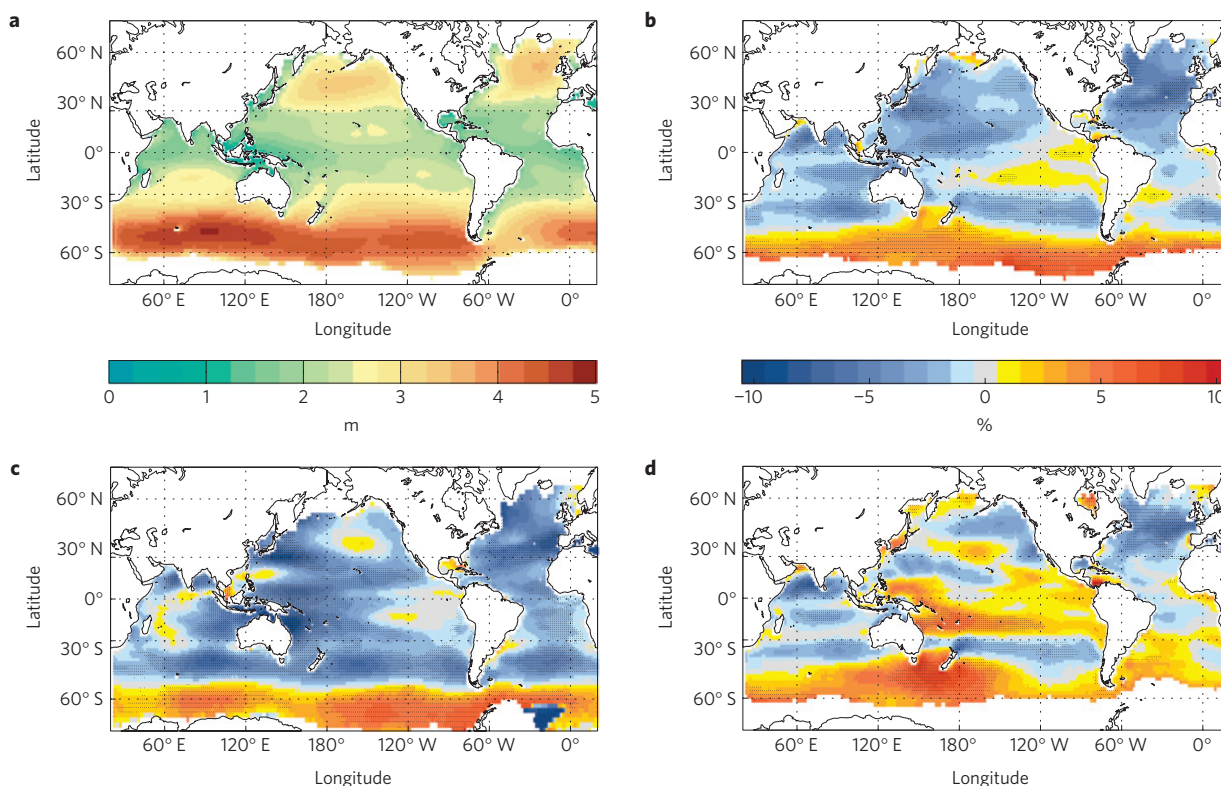


**Figure 2 | Projected future changes in multi-model averaged significant wave height.** **a**, Averaged multi-model annual significant wave height ( $H_S$ , m) for the time-slice representing present climate (~1979–2009). **b–d**, Averaged multi-model projected changes in annual (**b**), JFM (**c**) and JAS (**d**) mean  $H_S$  for the future time-slice (~2070–2100) relative to the present climate time-slice (~1979–2009) (% change). Stippling denotes areas where the magnitude of the multi-model ensemble mean exceeds the inter-model standard deviation. Results for individual models are included in the Supplementary Information.

**Table 1 | Percentage area of global ocean where projected increase/decrease is robust within the multi-model ensemble.**

	Annual		JFM		JAS	
	Percentage area of robust projected increase	Percentage area of robust projected decrease	Percentage area of robust projected increase	Percentage area of robust projected decrease	Percentage area of robust projected increase	Percentage area of robust projected decrease
$H_S$	7.1	25.8	4.9	38.5	8.8	8.4
$T_M$	30.2	19.0	8.7	44.6	33.6	10.7
$\theta_M$	18.4	19.7	8.95	21.4	17.1	12.7

See Methods for definition used for robustness. Increase (decrease) in direction ( $\theta_M$ ) corresponds to clockwise (anti-clockwise) rotation.

strengthening of the westerlies<sup>17</sup>. Small areas of projected increase in the tropical eastern Pacific Ocean are associated with an increasing Southern Ocean swell component (substantiated by increasing  $T_M$ —see below). An agreed decrease in  $\bar{H}_S$  across all models is projected in all other ocean basins, particularly in the subtropics. In the North Atlantic, this decrease spans all seasons, generally consistent with projected wind changes in the Coupled Model Intercomparison Project, Phase 3 (CMIP3; ref. 18) multi-model data set<sup>9</sup>. In the boreal winter (JFM; Fig. 2c), the relative area of projected decrease is enhanced (38.5% (4.9%) of oceans show projected decrease (increase); Table 1). In the austral winter however (JAS; Fig. 2d), regions of projected decrease and increase are comparable at about 8% of the global ocean (Table 1). A notable region of agreed projected increase is observed in the southern Pacific trade wind zone, consistent with projected strengthening of easterly trade winds in the winter subtropics seen in the CMIP3 multi-model data set<sup>19</sup>.

Although the area of projected  $H_S$  increase is relatively limited in extent (to the Southern Ocean), the projected increase in  $T_M$  over a much larger area (30.2 % of the global ocean shows an increase in annual mean  $T_M$ ; Table 1 and Fig. 3) shows the extended influence of enhanced Southern Ocean wave generation propagating as swell northwards across the global ocean. This Southern Ocean influence on  $T_M$  is large during the austral winter (33.6% of the global ocean shows a robust projected increase in JAS mean  $T_M$ ; Table 1), but not during the boreal winter (44.6% of the global ocean shows a robust projected decrease in JFM mean  $T_M$ ; Table 1).

Shoreline position is equally sensitive to directional changes as to changes in wave height<sup>20</sup>. Projected anticlockwise rotations of  $\theta_M$  (Fig. 4) are predominantly located on the northern side of the extratropical storm belts (westerly regions) in the Southern Ocean, North Pacific and Atlantic basins (19.7%, 21.4% and 12.7% of the global ocean in annual, JFM and JAS means, respectively). These correspond with an increased southerly component of  $\theta_M$

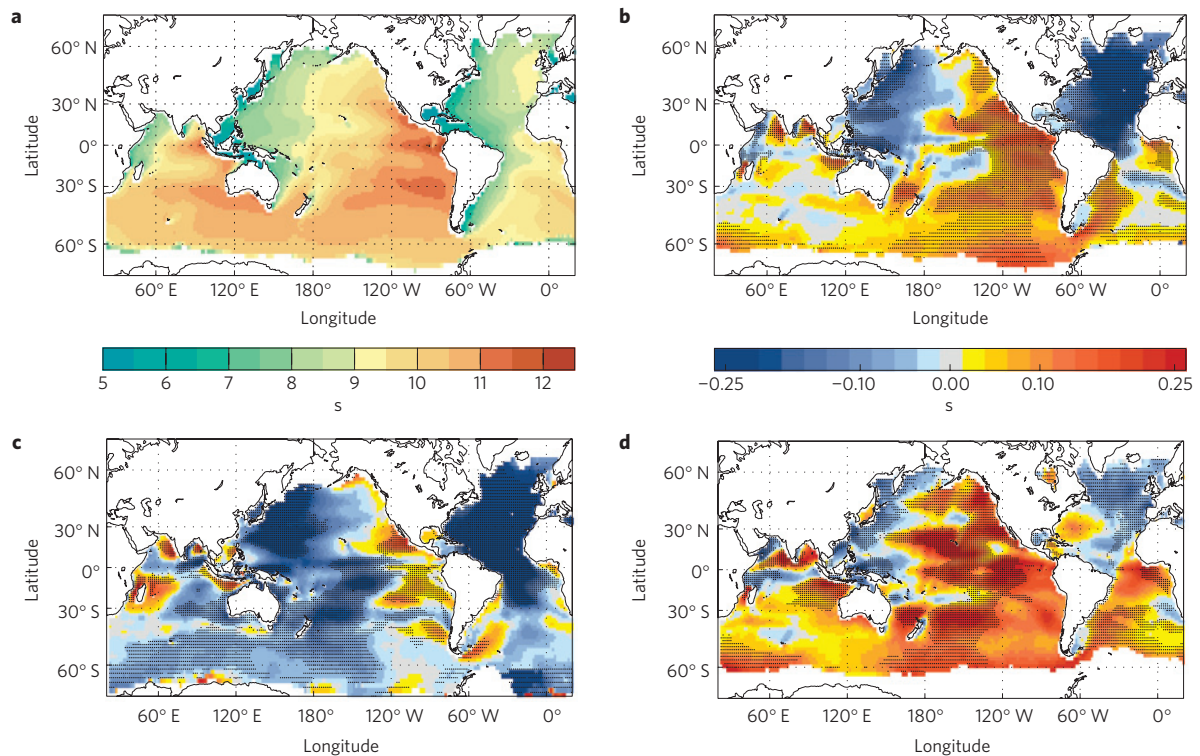


**Figure 3 | Projected future changes in multi-model averaged mean wave period.** **a**, Averaged multi-model annual mean wave period ( $T_M$ , s) for the time-slice representing present climate ( $\sim 1979\text{--}2009$ ). **b–d**, Averaged multi-model projected changes in annual (**b**), JFM (**c**) and JAS (**d**) mean  $T_M$  for the future time-slice ( $\sim 2070\text{--}2100$ ) relative to the present climate time-slice ( $\sim 1979\text{--}2009$ ) (absolute change, seconds). Mean wave period from only two groups is used (HEA12 and FEA12). Stippling denotes areas where the two models agree on the sign of change. Results for individual models, including MEA10, are included in the Supplementary Information.

associated with projected poleward shifts of the storm tracks<sup>17</sup>. In the southern equatorial region, the projected clockwise rotation in  $\theta_M$  is associated with more southerly wind waves. In the northern equatorial region, the projected clockwise rotation is associated with more easterly wind waves. Both features are consistent with a larger contribution of Southern Ocean swell.

A seasonal signal of projected changes in  $\theta_M$  is observed in the equatorial Pacific. In the boreal winter (JFM; Fig. 4b), anticlockwise rotation (up to  $10^\circ$ ) of the waves generated by the easterly trade wind in the northern equatorial Pacific infers an increased northerly component (propagating away from the northern extratropical storm belt). In the austral winter (JAS; Fig. 4c), a projected anticlockwise rotation in the southern equatorial Pacific suggests an increased southeasterly component, consistent with projected strengthening of trade winds in the region associated with stronger projected sea-surface temperature increase on the Equator relative to the South Pacific<sup>21</sup>.

Features of projected change in wave climate observed in our study are consistent with a broader understanding of wave-climate variability as a response to projected changes in atmospheric circulation. See Supplementary Information for a discussion on the changes in climate regimes that are potentially responsible for the dominant features of projected wave-climate change.

A range of projected scenarios is evident within the ensemble (see Supplementary Information) owing to the many levels of uncertainties in future wave-climate projections that stem from different sources, introduced at various stages in the modelling process. Our data set is best described as an ensemble of opportunity and it is recognized that extracting policy-relevant information and quantifying uncertainties from such a data set is difficult<sup>22</sup>. Our ensemble presents many challenges, in that it is too limited to sample the full range of uncertainty. Simulations within the ensemble

span different forcing scenarios, GCMs, downscaling and wave modelling approaches, insufficiently sampled to resolve dominant sources of variance. Limited analysis (see Supplementary Information) suggests the dominant source of variance of projected wave-climate change in the available studies is a function of methodology. WS06 (ref. 12) found the uncertainty due to differences among three climate models they assessed was much larger than that due to differences among the three forcing scenarios considered. From this study, we suggest the third level of uncertainty they discussed but did not quantify (that is, the uncertainty due to different approaches taken to generate regional-scale climate-change information from global climate model simulations, such as the use of different regional climate models, or dynamical versus statistical downscaling approaches, or different statistical approaches) is greater than forcing and model uncertainties.

The present ensemble of wave-climate projections was derived from CMIP3 GCM simulations. The low temporal and spatial resolution archives from CMIP3 had limited application for wind-wave studies. CMIP5 (ref. 23) provides a data set that will enable improved systematic sampling of uncertainty in wave-climate projections. Although the wave-climate community is hopeful, it remains to be seen whether CMIP5-derived projections will enable sources of variance within the wind-wave ensemble to be better quantified.

Until recently, coastal impacts of climate-change studies have been preoccupied with the influence of sea-level rise. There is a need to determine how other driving forces in the coastal zone (for example, waves and storm surges) will respond to a changing climate to aid these studies. Here, we have shown that wave climate is projected to change over large areas of the global ocean in a future climate, but a broad range of uncertainty surrounds these projections dominated by downscaling methodologies. Storm surge

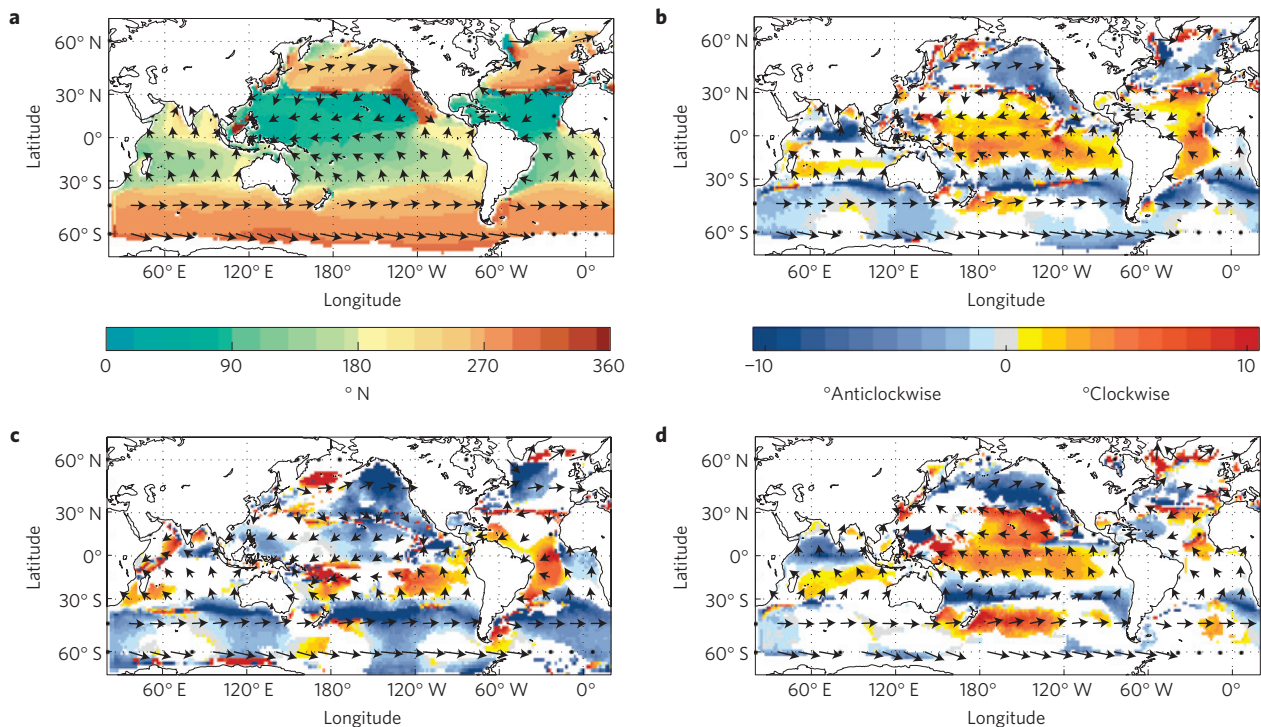


**Figure 4 | Projected future changes in multi-model averaged mean wave direction.** **a**, Averaged multi-model annual mean wave direction ( $\theta_M$ , ° N) for a historical time-slice (~1979–2009). The vectors indicate the directions shown in the left colour bar. **b–d**, Averaged multi-model projected changes in annual (**b**), JFM (**c**) and JAS (**d**) mean wave direction ( $\theta_M$ ) for a projected time-slice (~2070–2100) relative to historical climate (absolute change, ° clockwise). The vector direction denotes  $\theta_M$  for the historical time-slice. Colour denotes the magnitude of projected change according to the right colour bar. Mean wave directions from three groups are used (HEA12, MEA10 and FEA12). Only areas where groups agree on the sign of change are coloured. Results for individual models are included in the Supplementary Information.

climate projections probably exhibit these same characteristics. Interannual variability of waves and surges is a dominant source of shoreline position variance<sup>24</sup>, in some cases exceeding the influence of projected sea-level rise<sup>20</sup>. Low confidence in projected changes of wind-wave characteristics (height, length and directions) casts considerable doubt on the very-high-confidence categorization that coasts will be exposed to increasing risk in a future climate<sup>25</sup>.

## Methods

Monthly mean  $H_S$ , mean wave period,  $T_M$ , and mean wave direction  $\theta_M$ , were obtained from each wave-climate projection data set (Supplementary Table SM2). The only parameter common to all data sets is the monthly mean  $H_S$  (20 ensemble members), and this parameter is the focus of the intercomparison. However, climate-change-driven impacts (offshore and/or in the coastal zone) will also probably result from changes in  $T_M$  and  $\theta_M$ .  $T_M$  is available from 2 studies (4 ensemble members), and  $\theta_M$  is available from 3 studies (5 ensemble members). The projected change in these limited ensembles for these wave parameters is also considered.

For each data set, annual and seasonal (JFM and JAS) means of a given wave parameter are determined from the archive of monthly values for each of the present and projected time-slices. We note discrepancies in the definition of present wave climate between studies (for example, the SEA12 present time-slice, 1959–1990, differs considerably from other studies, which have a common period 1979–2004). To aid intercomparison between studies, we assume that differences between studies for the present climate are attributable to model error, and not from non-stationarity of the wave climate.

Model skill for the present wave climate is assessed by comparison with wave fields obtained from ERA-Interim<sup>15</sup> (1979–2009) and statistically corrected ERA-40 (ref. 16; C-ERA40, 1979–2002) reanalyses. A low bias in ERA-40  $H_S$  (ref. 26) was reported in ref. 16, in which the statistically corrected  $H_S$  (C-ERA40) data set used in this study was developed. Dynamical biases in  $T_M$  and  $\theta_M$  remain in the ERA-40 data, and we do not include these data in our study. Furthermore, owing to the general scarcity of wave data, an assimilative wave reanalysis will strongly depend on the background model, and will never be data-dominated and thus the error statistics of such a reanalysis are inhomogeneous, and cannot be estimated effectively. Annual and seasonal mean values of  $H_S$ ,  $T_M$  and  $\theta_M$  are determined for

the present climate at 1.5° spatial resolution from the 6-hourly archives. Climate model wave fields are interpolated onto the ERA-Interim/C-ERA40 grid before calculating r.m.s.d. and spatial correlation coefficients for each variable ( $H_S$ ,  $T_M$  and  $\theta_M$ ) as simple measures of comparing model performance. Correlation and r.m.s.d. are calculated for each model over the present time-slice against ERA-Interim and C-ERA40 globally (G), over the regions north of 30° N (NH), between 30° N and 30° S (Eq) and south of 30° S (SH) for annual and seasonal—January–March (JFM) and July–September (JAS)—means (Fig. 1).

Changes in  $H_S$  statistics between the two (present and future) time-slices are calculated as percentage changes. Projected  $T_M$  changes are calculated as absolute values, and changes in  $\theta_M$  are calculated as clockwise or anticlockwise rotation in degrees relative to the present climate mean. A multi-model mean projected change is determined. Fourteen statistical projected scenarios are available from WS06, whereas other groups contributing dynamical projections consist of just one or two projected scenarios. Hence, a uniformly weighted mean across all projected scenarios would be inappropriately weighted to the statistical projections<sup>22</sup>. The provision of wave-climate projections is in a preliminary phase, and metrics for model performance are not well established. Consequently, our objective was to limit weighting or ranking of any existing study over any other. The full ensemble was therefore reduced to 5 members, with each member consisting of the average from a given study (for example, the 14-member WS06 ensemble was reduced to a single member). This choice was made on the basis that model skill depended strongly on method (or group from which the wave field originated). Figure 1 shows clustering of results dependent on their origin. Furthermore, analysis of projected change from all individual ensemble members shows strong similarity dependent on their origin (see Supplementary Information).

For mean  $H_S$  (available from all groups), the map of mean projected change is obtained as the 5-member multi-model mean difference between projected and present climate wave fields. Stippling is shown where the multi-model mean response exceeds the model spread (measured as one standard deviation across the 5 members) as a simple measure of model agreement (Fig. 2). Distribution of means is unavailable from all studies, prohibiting a more sophisticated approach<sup>27</sup>. For other parameters that were unavailable from all groups, the multi-model mean response was determined from fewer members (2 or 3 depending on variable). In these cases, stippling as a measure of model agreement is shown where all models agree on the sign of change (Figs 3 and 4). For annual and seasonal means of each wave variable, the percentage area of the global ocean that exhibits agreed (by the above definitions) projected increase and decrease was determined (Table 1).

Received 23 May 2012; accepted 22 November 2012;  
published online 13 January 2013

## References

- Lowe, J. A. *et al.* in *Understanding Sea-Level Rise and Variability* (eds Church, J. A. *et al.*) 326–375 (Wiley-Blackwell, 2011).
- Hemer, M. A., Wang, X. L., Church, J. R. & Swail, V. R. Coordinating global ocean wave climate projections. *Bull. Am. Meteorol. Soc.* **91**, 451–454 (2010).
- Woolf, D. K., Challenor, P. G. & Cotton, P. D. Variability and predictability of the North Atlantic wave climate. *J. Geophys. Res.* **107**, 3145 (2002).
- Hemer, M. A., Church, J. A. & Hunter, J. R. Variability and trends in the directional wave climate of the Southern Hemisphere. *Int. J. Climatol.* **30**, 475–491 (2010).
- Semedo, A., Suselj, K., Rutgersson, A. & Sterl, A. A global view on the wind sea and swell climate and variability from ERA-40. *J. Clim.* **24**, 1461–1479 (2011).
- Young, I. R., Zieger, S. & Babanin, A. V. Global trends in wind speed and wave height. *Science* **332**, 451 (2011).
- Gulev, S. K. & Grigorieva, V. Last century changes in ocean wind wave height from global visual wave data. *Geophys. Res. Lett.* **31**, L24302 (2005).
- Tokinaga, H. & Xie, S.-P. Wave- and anemometer-based sea surface wind (WASWind) for climate change analysis. *J. Clim.* **24**, 267–285 (2011).
- McInnes, K. L., Erwin, T. A. & Bathols, J. M. Global climate model projected changes in 10 m wind speed and direction due to anthropogenic climate change. *Atmos. Sci. Lett.* **12**, 325–333 (2011).
- Cavaleri, L., Fox-Kemper, B. & Hemer, M. Wind-waves in the coupled climate system. *Bull. Am. Meteorol. Soc.* **93**, 1651–1661 (2012).
- Hemer, M. A., Wang, X. L., Weisse, R. & Swail, V. R. Community advancing wind-waves climate science: The COWCLIP project. *Bull. Am. Meteorol. Soc.* **93**, 791–796 (2012).
- Wang, X. L. & Swail, V. R. Climate change signal and uncertainty in projections of ocean wave heights. *Clim. Dynam.* **26**, 109–126 (2006).
- Mori, N., Yasuda, T., Mase, H., Tom, T. & Oku, Y. Projection of extreme wave climate change under the global warming. *Hydrol. Res. Lett.* **4**, 15–19 (2010).
- Hemer, M. A., Katzfey, J. & Trenham, C. Global dynamical projections of surface ocean wave climate for a future high greenhouse gas emission scenario. *Ocean Modelling* <http://dx.doi.org/10.1016/j.ocemod.2012.09.008> (2012).
- Dee, D. P. *et al.* The ERA-Interim reanalysis: Configuration and performance of the data assimilation system. *Q. J. R. Meteorol. Soc.* **137**, 553–597 (2011).
- Sterl, A. & Caires, S. Climatology, variability and extrema of ocean waves—The web-based KNMI/ERA-40 wave atlas. *Int. J. Climatol.* **25**, 963–997 (2005).
- Arblaster, J. M., Meehl, G. A. & Karoly, D. J. Future climate change in the Southern Hemisphere: Competing effects of ozone and greenhouse gases. *Geophys. Res. Lett.* **38**, L02701 (2011).
- Meehl, G. A. *et al.* The WCRP CMIP3 multi-model dataset: A new era in climate change research. *Bull. Am. Meteorol. Soc.* **88**, 1383–1394 (2007).
- Sobel, A. H. & Camargo, S. J. Projected future changes in tropical summer climate. *J. Clim.* **24**, 473–487 (2011).
- Coelho, C., Silva, R., Veloso-Gomes, F. & Taveira-Pinto, F. Potential effects of climate change on northwest Portuguese coastal zones. *ICES J. Mar. Sci.* **66**, 1497–1507 (2009).
- Timmermann, A., McGregor, S. & Jin, F.-F. Wind effects on past and future regional sea level trends in the southern Indo-Pacific. *J. Clim.* **23**, 4429–4437 (2010).
- Knutti, R., Furrer, R., Tebaldi, C., Cermak, J. & Meehl, G. Challenges in combining projections from multiple climate models. *J. Clim.* **23**, 2739–2758 (2010).
- Taylor, K., Stouffer, R. & Meehl, G. A. An overview of CMIP5 and the experiment design. *Bull. Am. Meteorol. Soc.* **93**, 485–498 (2012).
- Kuriyama, Y., Banno, M. & Suzuki, T. Linkages among interannual variations of shoreline, wave and climate at Hasaki, Japan. *Geophys. Res. Lett.* **39**, L06604 (2012).
- Nicholls, R. J. *et al.* in *IPCC Climate Change 2007: Impacts, Adaptation and Vulnerability* (eds Parry, M. L., Canziani, O. F., Palutikof, J. P., van der Linden, P. J. & Hanson, C. E.) 315–356 (Cambridge Univ. Press, 2007).
- Uppala, S. *et al.* The ERA-40 re-analysis. *Q. J. R. Meteorol. Soc.* **131**, 2961–3012 (2005).
- Tebaldi, C., Arblaster, J. M. & Knutti, R. Mapping model agreement on future climate projections. *Geophys. Res. Lett.* **38**, L23701 (2011).

## Acknowledgements

The study was conceived as part of the COWCLIP (ref. 4) project, an international collaborative working group endorsed by the World Climate Research Program and the Joint Commission on Oceanography and Marine Meteorology of the World Meteorological Organization and the UNESCO Intergovernmental Oceanographic Commission. We acknowledge the European Centre for Medium Range Weather Forecasting for the reanalysis data, and the climate modelling groups, the Program for Climate Model Diagnosis and Intercomparison (PCMDI) and the WCRP's Working Group on Coupled Modelling (WGCM) for their roles in making available the WCRP CMIP3 multi-model data set. Support of the CMIP3 data set is provided by the Office of Science, US Department of Energy. M.A.H. acknowledges the support of the Australian Climate Change Science Programme and the CSIRO Wealth from Oceans National Research Flagship. We thank all contributors to the COWCLIP project, along with J. Church for comments on an earlier version of the manuscript.

## Author contributions

All authors jointly conceived the study and contributed experimental data equally. M.A.H. analysed data and prepared the manuscript, with all authors discussing results and implications and commenting on the manuscript at all stages.

## Additional information

Supplementary information is available in the [online version of the paper](#). Reprints and permissions information is available online at [www.nature.com/reprints](http://www.nature.com/reprints). Correspondence and requests for materials should be addressed to M.A.H.

## Competing financial interests

The authors declare no competing financial interests.